nature nanotechnology

LETTERS

PUBLISHED ONLINE: 1 FEBRUARY 2009 | DOI: 10.1038/NNANO.2008.418

Bottom-up growth of fully transparent contact layers of indium tin oxide nanowires for light-emitting devices

C. O'Dwyer[1]*, M. Szachowicz[2], G. Visimberga[2], V. Lavayen[3,4], S. B. Newcomb[5] and C. M. Sotomayor Torres[6,7]

Thin layers of indium tin oxide are widely used as transparent coatings and electrodes in solar energy cells[1], flat-panel displays[2,3], antireflection coatings[4], radiation protection[5] and lithium-ion battery materials[6], because they have the characteristics of low resistivity, strong absorption at ultraviolet wavelengths, high transmission in the visible[7], high reflectivity in the far-infrared and strong attenuation in the microwave region. However, there is often a trade-off between electrical conductivity and transparency at visible wavelengths for indium tin oxide and other transparent conducting oxides. Here, we report the growth of layers of indium tin oxide nanowires that show optimum electronic and photonic properties and demonstrate their use as fully transparent top contacts in the visible to near-infrared region for light-emitting devices.

In developing techniques to fabricate homogeneous one-dimensional (1D) nanostructures, researchers have sought to control shape, aspect ratio and crystalline arrangement[8–10], and recent improvements in synthetic methods[11–13] have led to the direct integration of functional nanostructures into nanoscale devices[14–16]. Indium tin oxide (ITO) is the most important transparent conducting oxide and is therefore used in a wide range of applications. However, to date it has enjoyed only limited success as an ohmic contact for light-emitting devices (LEDs) due to high resistivities and an unacceptable trade-off between electrical and optical characteristics. Moreover, the limited availability of materials with suitable refractive indices has prevented the implementation of optical components with high performance. Hence, the possibility of forming complex, multilevel branched structures[17] with optimized optical properties in a single-step, bottom-up growth regime would be a significant advance given their compatibility with optoelectronic device architectures.

We have developed a simple, reproducible and controllable molecular beam epitaxy (MBE) system for growing high-quality, uniphasic, branched ITO nanowires on silicon and oxidized silicon surfaces using indium and tin precursors in an oxygen atmosphere. The layers of nanowires have electrical and optical properties and can be grown over large areas (several cm^2). With a transparency greater than 80% in the visible and greater than 90% between 1.2 and 1.6 μm, the layers could outperform the standard NiCr top contacts used in Si/SiGe multiple-quantum-well (MQW) LEDs.

The main structural features of nanowire layer growth are shown in Fig. 1. The entire process occurs in one step: seeding, nucleation, growth, and progressive branch seeding and growth. The initial stage involves the seeding of the substrate. Oxidized In–Sn droplets then condense on the substrate (Fig. 1a), and seed subsequent nanowire growth (Fig. 1b; see also Supplementary Information, Figs S1 and S2). Each nanowire (backbone and branches) is terminated with a uniphasic seed crystal (Fig. 1c), and crystallographic precipitation leads to non-tapered homogeneous nanowire growth. High-resolution transmission electron microscopy (HRTEM) analysis of the nanowires shows a cubic structure (Fig. 1d), and SEM observations show a square cross-section for all nanowires, confirmed by the HRTEM data showing evidence of nanowire growth along [100]. SEM and focused ion beam milling of the seed–wire interface to remove the seed crystal (see Supplementary Information, Fig. S2) shows the expected square cross-section due to growth from the [100] faces of the cubic structure seed, further confirmed by HRTEM of the nanowire in Fig. 1d, where we observe equally spaced (002) and (020) interplanar distances of 0.506 nm, and also by X-ray diffraction (see Supplementary Information, Fig. S1) where the phase is identified to be cubic $(In_{1.875}Sn_{0.125})O_3$ with $a_0 = 1.0124$ nm. At the initial stages of growth, these nanowires typically have diameters of 8–20 nm and lengths of 40–500 nm. The energy dispersive X-ray (EDX) spectra of the nanowires (Fig. 1e) confirm that individual wires comprise In, Sn and O equivalent to 5.9 atom% of Sn inclusion in In_2O_3 (6.25% is the theoretical maximum for $(In_{1.875}Sn_{0.125})O_3$).

For an overview of the typical morphological variations as a function of growth rate and substrate temperature see Supplementary Information, Fig. S3. We report a distinct growth mode modification from compact (but rough and partially porous) layers to dendritic nanowire growth during deposition. Locally increased porosity is the main defect found in graded index porous layer growth by oblique angle deposition techniques; such problems are not encountered for dense, highly branched nanowire layers. No heterogeneous catalysts are required and we still observe extremely high-quality, defect-free nanowires comprising the layers. At very low deposition rates, porous ITO layers are found (see Supplementary Information, Fig. S4), but at higher deposition rates single-crystal nanowires are formed.

After optimization on both quartz and silicon substrates, the growth method was applied to corresponding $n–i–p^+$ Si/SiGe MQW device structures, also grown by MBE (Fig. 2; see also Supplementary Information, Fig. S5). The LEDs with the nanowire contact layer exhibit a forward-bias turn-on voltage of 0.55 V at an injection current of 10 mA at room temperature (Fig. 2c), which is a marked improvement over LEDs and quantum cascade lasers with

[1]Department of Physics, and Materials and Surface Science Institute, University of Limerick, Limerick, Ireland, [2]Tyndall National Institute, University College Cork, Cork, Ireland, [3]Departamento de Física, Universidad Técnica Federico Santa María, Valparaíso 2390123, Chile, [4]Área de Ciências Naturais e Tecnológicas, Centro Universitario Franciscano, 97010-032 Santa Maria, RS, Brazil, [5]Glebe Scientific Limited, Newport, Co. Tipperary, Ireland, [6]Institute for Research and Advanced Studies, ICREA, 08010 Barcelona, Spain, [7]Catalan Institute of Nanotechnology, Edifici CM7, Campus Universitat Autonoma de Barcelona, 08193 Bellaterra (Barcelona), Spain; *e-mail: colm.odwyer@ul.ie

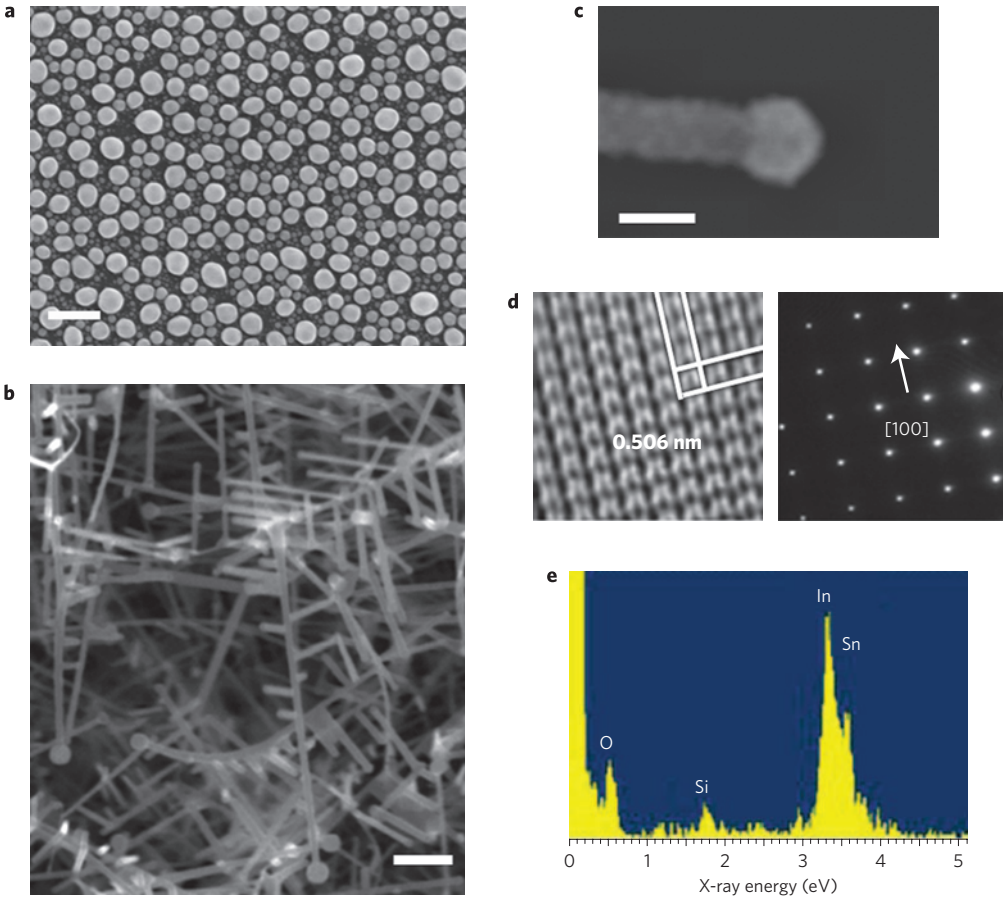

Figure 1 | ITO nanowire nucleation and growth. a, Plan-view SEM image of oxidized In–Sn droplet seed crystals under MBE deposition conditions of $T_{sub} = 400$ °C, $T_{In} = 835$ °C, $T_{Sn} = 1{,}000$ °C and at a rate of 0.1 nm s^{-1}. These seeds nucleate the precipitative growth of the nanowire. Scale bar, 100 nm. **b**, Cross-sectional SEM image of the interior of the nanowire layer grown at $T_{sub} = 400$ °C at nominal In : Sn (90 : 10) growth rates of 0.1 nm s^{-1}. Scale bar, 50 nm. **c**, SEM image of the faceted seed crystal–nanowire interface. **d**, The higher-magnification HRTEM image and associated selected-area electron diffraction pattern clearly identify the monocrystalline cubic $(In_{1.875}Sn_{0.125})O_3$ phase with (002) and (020) interplanar spacings of 0.506 nm. **e**, Large-area EDX spectrum of the nanowire layer showing the In and Sn L-edge lines, O and Si substrate lines.

oxidized Ni/Au, Ni/Cr or thin-film ITO/Ag/ITO sandwich contacts[3]. We conducted electrical measurements on a series of nanowire-containing segments using corner contacts to areas of the nanowire layer in the van der Pauw geometry[18]. The conductivity of the pure $(In_{1.875}Sn_{0.125})O_3$ branched nanowires is typically measured to be 1,053.5 $\pm$ 42.3 S cm^{-1} at room temperature, which is similar to the values previously reported for other individual nanowires and two orders of magnitude greater than individual In_2O_3 or SnO_2 nanowires[2]. Note that our conductivity values are similar to those reported previously[16] for Sn-doped (5–8 atom%) In_2O_3 nanowires, whereas that of In_2O_3 nanowires without intentional doping is of the order of 1 S cm^{-1}. The as-deposited nanowire layer exhibits a linear electrical behaviour even without the need for prior annealing or a metallic interlayer to curb high contact resistances, indicating a good ohmic contact (Fig. 2c, inset). An advantage of the nanowire morphology chosen in this case is that the spherical seed prevents unwanted field emission known to occur for sharp-tipped ITO nanowires[19]. Thus, by choosing a medium temperature of 575 °C, we can optimize the values for sheet resistance to over four orders of magnitude lower than currently available for known transparent conducting oxides.

Nanowire layer capacitance measurements were conducted using a capacitance bridge technique[20] to determine the field-effect mobilities and free carrier densities as a function of oxygen pressure (Fig. 2d). Oxidative crystallization of the ITO with increasing oxygen pressure contributes to the increased mobilities and carrier densities. The mobilities of the present nanowire layers are typically 55–65 cm^2 V^{-1} s^{-1} for oxygen pressures in the range 2×10^{-4} to 4×10^{-4} mbar and are comparable to In_2O_3 nanowires on oxide dielectrics ($\mu = 7$–280 cm^2 V^{-1} s^{-1}) and bulk monocrystalline In_2O_3 ($\mu = 160$ cm^2 V^{-1} s^{-1}) (ref. 21).

As mentioned above, the growth rate and temperature are key parameters in the eventual morphology of the ITO nanowire layers. To assess this influence on the optical transmission, ITO layers of varied thickness and morphology were grown on quartz substrates. Figure 3a shows their transmission spectra in the wavelength range 400–1,600 nm. The inset shows a typical ITO nanowire layer deposited on a glass cover slip. The transparency in the visible range improves to ~90% with increasing growth rate up to 0.2 nm s^{-1}. Spectroscopic ellipsometric measurements show the effective refractive indices of the nanowire layer–air interface to be between 1.04 and 1.12 for all samples investigated, directly due to the varied porosity of the nanostructured layers, calculated using the Bruggemann effective medium approximation. This is advantageous, as previous efforts to couple high transmission and low resistivity resorted to ITO/Ag/ITO multilayer sandwiches to combine the improved conductivity of Ag and the high refractive index of the ITO ($\eta = 2.19$) to boost the transmittance of the metal interlayer[6,22]. The measured absorption edge for the nanostructured ITO films is ~380 nm, a value lower than that for ITO on glass and comparable to ITO/YSZ (yttria-stabilized zirconia) lattice-matched thin films and nanowires[19].

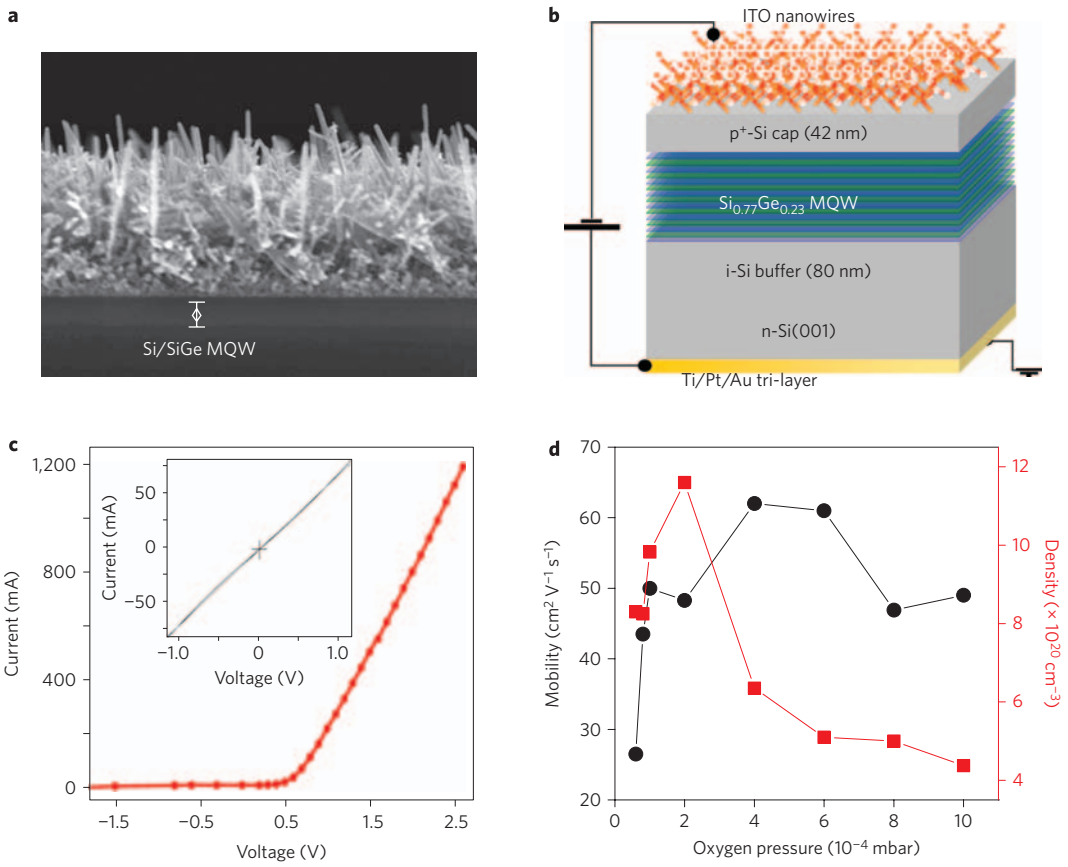

Figure 2 | Electrical characterization of ITO nanowire/SiGe MQW contacts. a, Cross-sectional SEM images of the nanowire layer on a SiGe MQW. The nanowire layer shown was grown at a substrate temperature of $T_{sub} = 575$ °C at a growth rate of 0.2 nm s^{-1} and an invariant oxygen partial pressure of 2.1×10^{-4} mbar. **b**, Schematic representation of the ITO nanowire contacted SiGe MWQ LED. The active region consists of a 15-period $Si/Si_{0.77}Ge_{0.23}/Si$ multiple quantum-well layer. The bottom contact is a Ti/Pt/Au trilayer. The nanowires were grown directly onto the p^+-Si. **c**, Room-temperature (295 K) *I*–*V* characteristics of the Si/SiGe MQW LED acquired in the absence of illumination. Inset: *I*–*V* characteristics of the ITO/p-Si ohmic contact. **d**, Free-carrier field-effect mobility (black circles) and density (red squares) of the ITO nanowires as a function of oxygen pressure during growth. The nanowires examined were grown at a rate of 0.2 nm s^{-1} at $T_{sub} = 575$ °C, $T_{In} = 835$ °C, $T_{Sn} = 1{,}000$ °C.

The calculated reflectivity at near-normal incidence (10°) as a function of wavelength was determined for the ITO nanowire layer (Fig. 3b), a porous ITO layer (see Supplementary Information, Fig. S4), a thin ITO film, and a standard antireflection layer of ITO on glass. ITO nanowire layers on silicon exhibited much lower reflectivity than either dense ITO on silicon or porous ITO layers in the wavelength region of interest. Only anti-reflection ITO coatings on glass showed similar transmission between 850 and 975 nm, but with an unacceptable sheet resistivity of ~15 Ω cm. Fresnel reflection associated with higher-refractive-index ITO thin films is virtually eliminated[23] due to reduction in the refractive index from the substrate to the nanowire layer/ambient interface, where the refractive index was measured to vary from 2.19 (close to the substrate) to 1.04 (at the air interface). The low-refractive-index nanowire layer is optically specular and exhibits a 'dark' surface (see Fig. 3a), confirming the absence of Fresnel reflection over a broad spectral width. This is particularly important for LED applications because of the isotropic emission from the active region and the fact that reflection phenomena can limit the light-extraction efficiency.

Typically, ITO and other transparent conducting oxides fail to transmit light in the near-infrared region above ~1.1 μm, thus preventing their use as electrodes for LEDs operating in the second (1.3 μm) and third (1.55 μm) optical communications energy windows. This is due to the onset of a metal-like behaviour at low photon energies, where quanta of incident electromagnetic radiation can couple to plasma oscillations. The surface plasmon resonance of ITO (determined using the Drude free-electron model and three-phase Fresnel equations of reflection) is observed at a much lower energy than for metals (where it generally falls into the visible range)[7]. In Fig. 3b, the surface plasmon resonance of the ITO nanowire layer (6,895 cm^{-1}) compared to a thin ITO film (10,204 cm^{-1}) is redshifted by ~480 nm, pushing the onset of reflectance further towards the near- to mid-infrared. The minimum in reflectivity is routinely observed in the crucial 1.2–1.6 μm range at near-normal incidence (0–10°). Angle-resolved reflectance measurements (see Supplementary Information, Fig. S6) conclusively show that the position of the surface plasmon resonance blueshifts with increasing angle; the window for maximum transmission over the widest wavelength range is observed near normal to the surface. Their suitability to silicon-based LEDs is demonstrated by measurements of the room-temperature electroluminescence emission from the nanowire-contacted SiGe MQW LED, which show unambiguously that the Si and SiGe emission lines are fully resolved through the nanowire layer contact in ambient laboratory conditions (Fig. 3c).

The low-temperature photoluminescence spectrum of the uncoated structure is shown in Fig. 4a. We observe the standard SiGe no-phonon- ($SiGe^{NP}$) and the SiGe transverse optical phonon-assisted ($SiGe^{TO}$) emission lines separated by ~56 meV (ref. 24). The lower curve in Fig. 4a was recorded from the structure contacted with 30 nm NiCr. We observe the photoluminescence

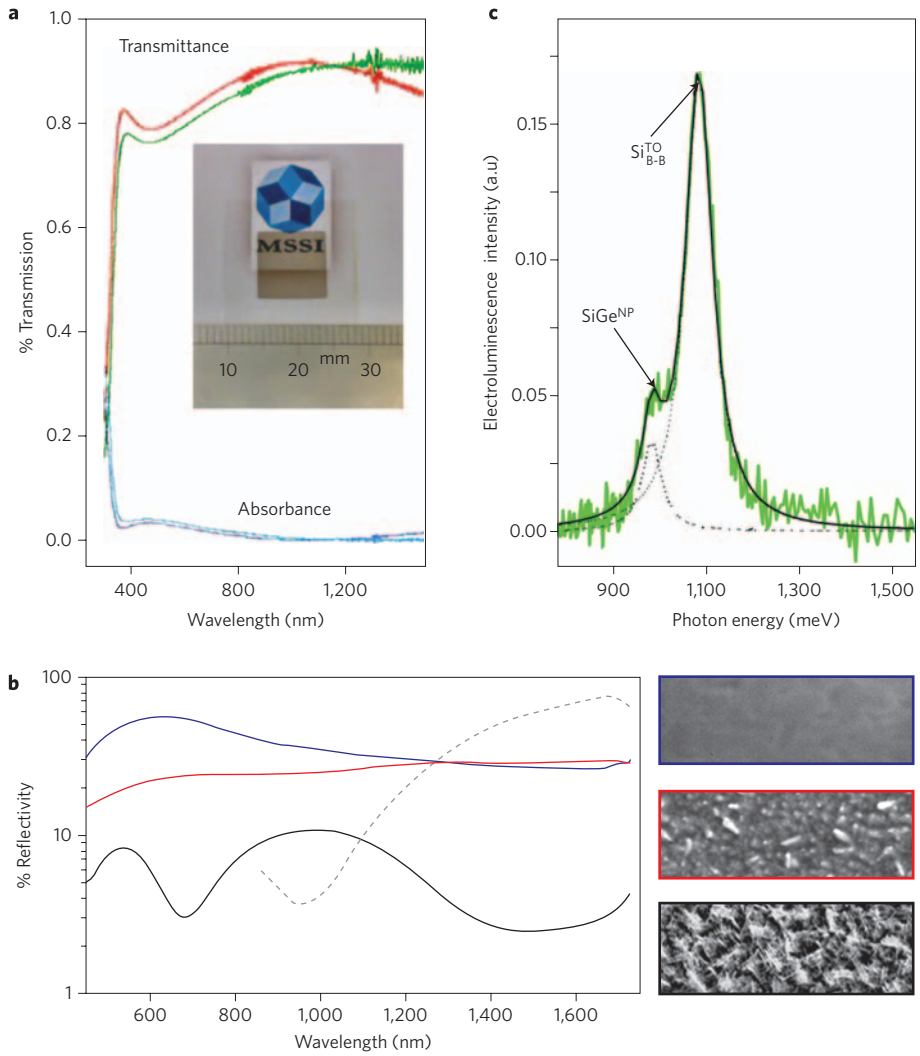

Figure 3 | Optical transmission characteristics of ITO nanowire layers. a, Transmission measurements of an ITO nanowire layer deposited at substrate temperatures of $T_{sub} = 575\ ^{\circ}C$ (red curve) and 450 °C (green curve) at a nominal growth rate of 0.05 nm s^{-1} and an invariant oxygen partial pressure of 2.1×10^{-4} mbar. The inset shows an ITO nanowire layer deposited on a glass cover slip. **b**, Reflectance spectra for a thin ITO antireflection coating (blue curve), a porous ITO layer (red curve) an ITO nanowire layer (all on silicon, black curve) and a thin ITO film on glass (dashed curve). Plan-view SEM images of each layer are also shown. **c**, Room-temperature (295 K) electroluminescence spectrum from an ITO nanowire-contacted Si/SiGe MQW structure acquired at an injection current of 575 mA. The $SiGe^{NP}$ (no phonon) and Si^{TO}_{B-B} (band-to-band transverse optical phonon) emission were extracted with a multiple Gaussian fit.

signal of the NiCr coated structure to be relatively weak, particularly for crucial excitonic recombinatorial routes. The photoluminescence intensity is attenuated in this case by ~97%, necessitating the use of a similar contact with high transmission in the wavelength range of use.

The corresponding comparative spectra of both the uncoated MQW and nanostructured ITO-contacted MQW are shown in Fig. 4b, where a marked improvement in transmission compared to the NiCr contacted MQW is observed. The highest attenuation was noted for the Si^{EHD} emission, although 20% of the uncoated MQW signal for this line was still transmitted, as opposed to negligible transmission through the NiCr contact. The Si^{TO}_{BE} emission was attenuated by ~50%, but of utmost interest are the SiGe emission lines, which were transmitted with negligible absorption. It is clear that the full spectrum (all important transitions) of a SiGe MQW LED can be resolved through the ITO nanowire top contact. Electroluminescence measurements as a function of temperature were also acquired from the ITO-contacted SiGe MQWs and are reproduced in Fig. 4c. The data indicate excellent temperature stability in the optoelectronic properties of the nanowire layer as a top contact. The SiGe band-edge electro- and photoluminescence can be detected up to room temperature and no saturation was observed even with injection current densities greater than 1,125 mA cm (electroluminescence) and at excitation power densities greater than 2,500 W cm^{-2} (photoluminescence) (see Supplementary Information, Fig. S7), indicating a very high diode quality with no electro-optical deterioration in the nanowire contacts.

Light, in this case the SiGe emission lines, escapes the nanowire layer due to its unusually low effective refractive index[25]. The escape cone for light in bulk ITO of refractive index $\eta = 2.19$ covers an effective solid angle (Ω) of 0.65 sr, given by $\Omega = 2\pi(1-\cos\omega)$ sr. The key to increasing the light escape probability is to allow multiple opportunities for photons to find the escape cone, emit and be detected. For the ITO nanowire layer with a refractive index of 1.04 for the nanowire layer–air interface, the solid angle for the escape cone increases to ~2.9 sr. This allows an efficient mechanism that redirects photons that were originally emitted out of the escape cone, back into the escape cone to boost external efficiency. The geometry of the nanowire layer maximizes transmission through a single-step, practical approach of randomizing scattering photons.

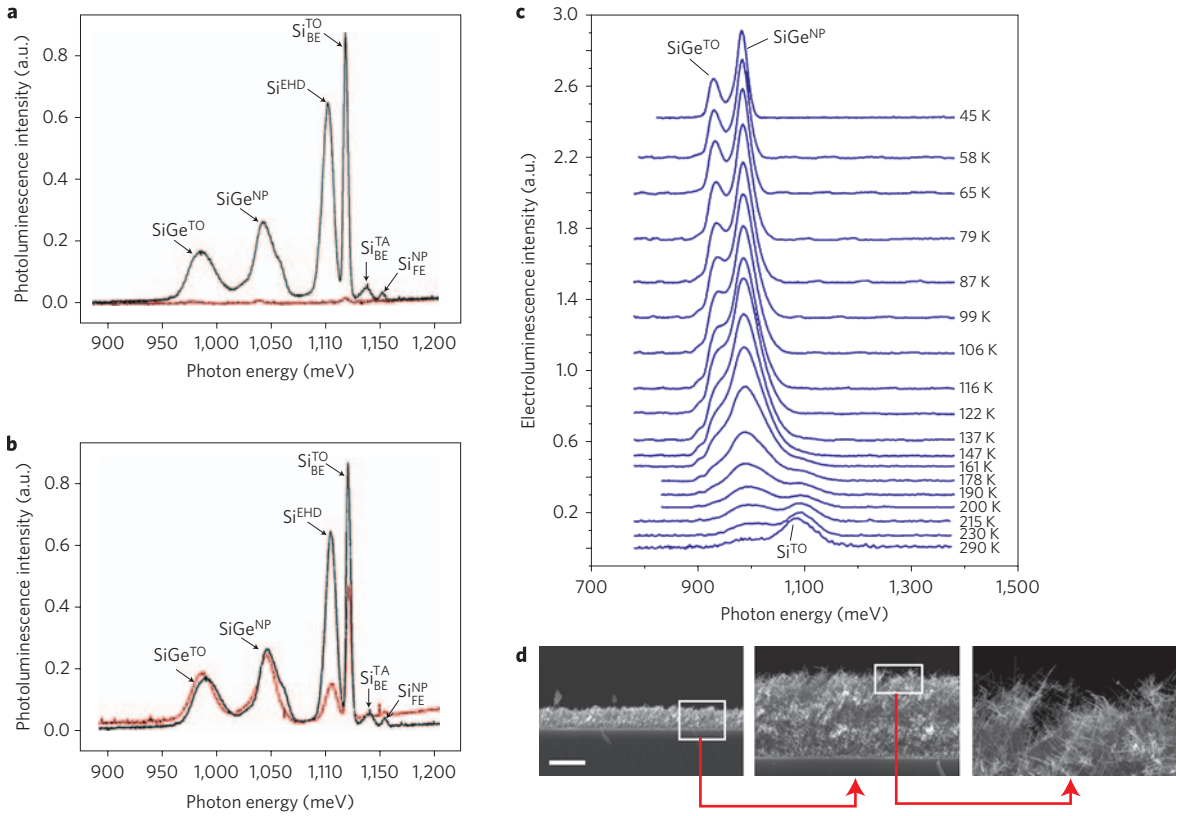

Figure 4 | Photo- and electroluminescence emission from ITO nanowire-contacted SiGe MQW LED. a,**b**, Comparison of the low-temperature (45 K) photoluminescence spectra of a non-contacted SiGe MQW (black curve) and a NiCr-contacted SiGe MQW (red curve) (**a**), a non-contacted SiGe MQW (black curve) and an ITO nanowire-contacted SiGe MQW (red curve) (**b**). The two high-intensity peaks observed at 1,125 and 1,150 nm correspond to the silicon transverse optical phonon-assisted bound exciton recombination (Si_{BE}^{TO}) and the silicon electron–hole droplet emission (Si^{EHD}), respectively. **c**, Temperature-dependent electroluminescence spectra from the Si/SiGe MQW acquired at a constant driving current of 575 mA in the range 45–295 K. The supplied power causes device heating, thus limiting the lowest temperature to ~45 K inside the cryostat. Luminescence is preserved up to room temperature. **d**, The series of SEM images of the nanowire layer highlights the overall long areal range uniformity of growth into dedicated fully transparent contact layers. The scale bar on the first image represents 1 μm. Each successive image (boxed region) was acquired with a magnification increase of ×4. These ITO nanowires have average cross-sectional diameters of 10–15 nm.

In addition, the emission is maximized by the angular dependence of the plasma frequency, where the transmission is both maximized and limited to near-normal output. As a whole, the optical and electrical properties are unique for any conductive, transparent oxide and have the added benefit of being experimentally more simple than the multi-step deposition of several defect-free layers of reducing refractive index (exhibiting poor conductivities) and highly conducting thin films (exhibiting poor transmission in the visible region).

Thus, the ability to fabricate monocrystalline and transparent doped metal-oxide nanowire layers with morphological control and phase homogeneity leads to excellent transparent top contacts to LEDs. The rational control of the one-step growth process allows the fabrication of nanowire layers over large areas without external catalysts, and with optimum electrical and optical characteristics. Modifications and extensions of the technique can be envisaged for similar materials, such as indium–zinc oxide and related compounds, and possibly for tuneable antireflection coatings.

Methods

Molecular beam epitaxial deposition and nanowire growth. Before ITO growth on silicon and glass substrates, and on Si/SiGe MQW structures, the respective surfaces were cleaned using a standard RCA process where the sample was immersed in a $H_2O_2 : NH_4OH:H_2O$ (1 : 1 : 1) solution at 80 °C for 30 min. After rinsing in deionized water, a second treatment was performed in a H_2O_2:HCl:H_2O (1 : 1 : 5) solution with subsequent rinsing in deionized water. Through this process, metallic and organic contamination was removed. In this last step, the surface was oxidized so that a thin (~7 nm) and clean SiO_2 layer formed at the surface. Dipping the sample in HF shortly before introducing it into the evaporator removed the oxide layer and passivated the surface with hydrogen. For evaporation of the In and Sn sources, a home-built MBE high-vacuum chamber with two distinct effusion cells for In and Sn together with an electron-beam evaporator, was designed in cooperation with MBE-Komponenten GmbH, with calibrated growth rates. During nanowire growth the sample surface was annealed at temperatures in the range 300–650 °C. The In:Sn (90 : 10) was evaporated at growth rates in the range 0.02–0.2 nm s^{-1} up to maximum temperatures for In and Sn of $T_{In} = 835$ °C, $T_{Sn} = 1{,}000$ °C, respectively.

For transparency studies, a glass control substrate was also mounted in the growth chamber in tandem with the Si/SiGe MQW. ITO nanowire layers deposited on glass were used to determine the sheet resistance and the transparency of a similar layer to that grown on the device. The growth parameters were chosen to achieve a transparency of at least 90% in the 1.2–1.6 μm SiGe emission range and sheet resistivities in the range 1×10^{-4} to 4×10^{-4} Ω cm. A substrate growth temperature $T_{sub} = 575$ °C gave a sheet resistivity of 1.7×10^{-4} Ω cm when both In and Sn were deposited at a rate of 0.2 nm s^{-1}.

Electron microscopy. The morphological characterization of the nanowire layers was performed by field-emission scanning electron microscopy using a Hitachi S-4800 operating at beam voltages between 5 and 30 kV. Electron transparent specimens were prepared by ion-milling techniques and placed on a holey carbon support. Transmission electron microscopy (TEM) and selected-area electron diffraction were conducted using a JEOL JEM-2000FX TEM operating at 200 kV and a Philips CM300 FEGTEM operating at 300 kV. Focused ion beam milling was conducted using a FEI 200 FIBSIMS Workstation.

X-ray diffraction. X-ray diffraction and reflectivity measurements were performed using a high-resolution X-ray diffractometer (Rigaku SLX-2000). A rotating anode Cu Kα source ($\lambda = 0.15418$ nm, 18 kW) was used and the X-ray beam was monochromatized using a channel-cut Ge(220) monochromator. The incident and

reflected beams were collimated with slits of 0.05 mm in width and the reflection intensity was measured with a scintillation counter.

Electro- and photoluminescence/reflectance measurements. Optical excitation came from a 6 W Argon ion (Ar^+) laser (Spectra Physics Stabilite 2017) operating at 514.5 nm. Luminescence was collected through a SPEX 1680 double monochromator into a cooled North Coast EO-817L Ge detector. For photoluminescence and electroluminescence measurements, a pulsed excitation optical signal with a fixed frequency of 590 Hz and an electrical signal pulsed at 570 Hz were used and modulated by a mechanical chopper. The output from the chopper was fed through a lock-in amplifier measuring the output signal of the Ge detector sensitive in a spectral range 0.8–1.7 μm. Reflectance measurements were carried out in a Bruker FT-IR spectrometer IFS66/V. Different configurations of beamsplitters, detectors and sources were used to cover the spectral range from far-infrared (10 cm^{-1}) to near-infrared and visible ranges. For angular resolved measurements, a NIR512 Ocean Optics spectrometer was used as a detector in a home-built reflectance/transmittance setup.

Comparative photo- and electroluminescence measurements were performed on Si/SiGe MQW LEDs grown by MBE. To compare the optical transmission, an ITO nanowire layer and a 30 nm NiCr metal contact were deposited on two separate samples on the same substrate. As a reference, the photoluminescence spectrum of an uncoated MQW structure was recorded under identical conditions.

Si/SiGe multiquantum-well LED and electrical characterization. The $n-i-p^+$ Si/SiGe multiquantum-well (MQW) structures were grown by MBE. On an 80 nm undoped Si buffer grown at 700 °C on Si(001), a 15-period $Si/Si_{0.77}Ge_{0.23}$ (4.1 nm/3.9 nm) quantum-well structure was deposited at 625 °C. The entire structure was capped with 42 nm B-doped (5×10^{18} cm^{-3}) Si to saturate SiGe dangling bonds. After an additional 10 nm Si top layer grown at 625 °C, a capping layer of 30 nm p^+–Si (p-doped) was grown at 700 °C. The back contact was a Ti (50 nm diffusion barrier)/Pt (50 nm)/Au (100 nm) multilayer ohmic contact. Several structures were top-contacted with a Ni/Cr bilayer deposited by sputtering. Electrical characterization was performed at room temperature under ambient conditions. Resistivity measurements were conducted using a four-point probe system (Jandel Engineering), and mobility measurements were acquired with a Andeen-Hagerling Model 2550A capacitance bridge and a BioRad Polaron Division Hall Measuring System HL5200. All current–voltage ($I-V$) measurements were conducted with a HP Semiconductor Parameter Analyzer 4145A.

Received 25 September 2008; accepted 23 December 2008; published online 1 February 2009

References

1. Ginely, D. S. & Bright, C. Transparent conducting oxides. *MRS Bull.* **25,** 15–65 (2000).
2. Wan, Q. *et al.* High-performance transparent conducting oxide nanowires. *Nano Lett.* **6,** 2909–2915 (2006).
3. Sawada, M., Higuchi, M., Kondo, S. & Saka, H. Characteristics of indium-tin-oxide/silver/indium-tin-oxide sandwich films and their application to simple-matrix liquid-crystal displays. *Jpn J. Appl. Phys.* **40,** 3332–3336 (2001).
4. Kim, H., Horwitz, J. S., Kim, W. H., Kafafi, Z. H. & Chrisey, D. B. Highly oriented indium tin oxide films for high efficiency organic light-emitting diodes. *J. Appl. Phys.* **91,** 5371–5376 (2002).
5. Synowicki, R. A., Hale, J. S., Ianno, N. J. & Woollam, J. A. Low earth orbit effects on indium tin oxide and polyester and comparison with laboratory simulations. *Surf. Coat. Technol.* **62,** 499–503 (1993).
6. Kim, D.-W. *et al.* Highly conductive coaxial SnO_2–In_2O_3 heterostructured nanowires for Li ion battery electrodes. *Nano Lett.* **7,** 3041–3045 (2007).
7. Granqvist, C. G. & Hultåker, A. Transparent and conducting ITO films: new developments and applications. *Thin Solid Films* **411,** 1–5 (2002).
8. Cui, Y. & Lieber, C. M. Functional nanoscale electronic devices assembled using silicon nanowire building blocks. *Science* **291,** 851–853 (2006).
9. Hsu, Y.-J. & Lu, S.-Y. Vapor–solid growth of Sn nanowires: Growth mechanism and superconductivity. *J. Phys. Chem. B* **109,** 4398–4403 (2005).
10. Zhou, J. *et al.* Vertically aligned Zn_2SiO_4 nanotube/ZnO nanowire heterojunction arrays. *Small* **3,** 622–626 (2007).
11. Lu, J. G., Chang, P. & Fan, Z. Quasi-one-dimensional metal oxide materials—Synthesis, properties and applications. *Mater. Sci. Eng. R* **52,** 49–91 (2006).
12. Johnson, M. C., Aloni, S., McCready, D. E. & Bourret-Courchesne, E. Controlled vapour–liquid–solid growth of indium, gallium and tin oxide nanowires via chemical vapor transport. *Cryst. Growth Des.* **6,** 1936–1941 (2006).
13. Nguyen, P. *et al.* Epitaxial directional growth of indium-doped tin oxide nanowire arrays. *Nano Lett.* **3,** 925–928 (2003).
14. Xiang, J. *et al.* Ge/Si nanowire heterostructures as high-performance field-effect transistors. *Nature* **441,** 489–493 (2006).
15. Law, M., Greene, L. E., Johnson, J. C., Saykally, R. & Yang, P. D. Nanowire dye-sensitized solar cells. *Nature Mater.* **4,** 455–459 (2005).
16. Dattoli, E. N. *et al.* Fully transparent thin-film transistor devices based on SnO_2 nanowires. *Nano Lett.* **7,** 2463–2469 (2002).
17. Wang, D. L. & Lieber, C. M. Inorganic materials: Nanocrystals branch out. *Nature Mater.* **2,** 355–356 (2003).
18. van der Pauw, L. J. A method of measuring specific resistivity and Hall effect of discs of arbitrary shape. *Philips Res. Repts.* **13,** 1–9 (1958).
19. Wan, Q., Feng P. & Wang T. H. Vertically aligned tin-doped indium oxide nanowire arrays: Epitaxial growth and electron field emission properties. *Appl. Phys. Lett.* **89,** 123102 (2006).
20. Zhang, L., Tu, R. & Dai, H. J. Parallel core–shell metal–dielectric–semiconductor germanium nanowires for high-current surround-gate field-effect transistors. *Nano Lett.* **6,** 2785–2789 (2006).
21. Nguyen, P. *et al.* Direct integration of metal oxide nanowire in vertical field-effect transistor. *Nano Lett.* **4,** 651–657 (2004).
22. Ju, S. *et al.* Fabrication of fully transparent nanowire transistors for transparent and flexible electronics. *Nature Nanotech.* **2,** 378–384 (2007).
23. Kim, J. K. *et al.* Light extraction enhancement of GaInN light emitting diodes by graded refractive index indium tin oxide anti-reflection contact. *Adv. Mater.* **20,** 801–804 (2008).
24. Weber, J. & Alonso, I. Near-band-gap photoluminescence of Si–Ge alloys. *Phys. Rev. B* **40,** 5683–5693 (1989).
25. Schnitzer, I., Yablonovitch E., Caneau, C., Gmitter, T. J. & Scherer, A. 30% external quantum efficiency from surface textured, thin-film light-emitting diodes. *Appl. Phys. Lett.* **63,** 2174–2176 (1993).

Acknowledgements

The authors acknowledge support from Science Foundation Ireland (02/IN.1/172) and the EU Network of Excellence nanoPhotonics to Realise Molecular Scale Technologies (PhOREMOST) (FP6/2003/IST/2-511616). V.L. thanks the Programa Bicentenario de Cienca y Tecnología (PBCT), Chile (ACT027) and Conselho Nacional de Desenvolvimento Cientifico e Tecnologico (CNPq), Brazil. We also acknowledge the contributions of N. Roos and T. P. Sidiki to the design of the MBE reactor, and thank A. C. Martín (Consejo Superior de Investigaciones Cientificas, CSIC) for MBE deposition of Ti/Pt/Au bottom contacts on selected samples, and D. Lebedev (University of Wuppertal) for ellipsometric characterization. We also thank C. Gergely and P. Arcade (Université Montpellier II) for access to their far-infrared spectrometer.

Author contributions

C.O.D., M.S. and C.M.S.T. conceived and designed the experiments and analyses. C.O.D., M.S. and G.V. performed the experiments. C.O.D., M.S., G.V. and V.L. analysed the data. S.B.N. conducted part of the TEM analysis and C.M.S.T. supervised the work. All authors discussed the results and C.O.D. wrote the manuscript.

Additional information

Supplementary Information accompanies this paper at www.nature.com/naturenanotechnology. Reprints and permission information is available online at http://npg.nature.com/reprintsandpermissions/. Correspondence and requests for materials should be addressed to C.O.D.